

6DoF Registration of 2D Laser Scans

Benjamin Huhle, Timo Schairer, Andreas Schilling, Wolfgang Straßer
Department of Graphical Interactive Systems (GRIS)
University of Tübingen
Tübingen, Germany
{huhle, schairer}@gris.uni-tuebingen.de

Abstract—We address the problem of registering a set of 2D laser scans in 3D space with regard to six degrees of freedom. Registering single 2D scans is only possible when making strong assumptions on the structure of the scene or on the acquisition process, since only a slice of the 3D environment is captured and the information content is very limited. With a combination of two differently oriented laser scanners, however, the registration problem becomes feasible. We present a method that is based on the idea of preserving the free space represented in each of these combined scans. On realistically simulated laser range data we show that, given a sufficient sampling density, the proposed algorithm is capable to recover from large translational and moderate rotational errors in the initial configuration.

Keywords—scan matching; registration; laser range finder

I. INTRODUCTION

For the acquisition and reconstruction of 3D models from an inside-looking-out perspective, such as models of indoor environments or densely structured city models it is necessary to move the acquisition device through the scene to accumulate views from different viewpoints in order to avoid occlusions. The acquisition of a single depth map with a 3D laser scanner (e.g. a sweeping 2D laser scanner), however, takes significant time. Contrarily, simple 2D scanners can work at very high frequency and a continuous form of scanning (in contrast to the so-called stop-scan-go pattern, that is mostly applied with 3D scanners) might be achievable more easily by registering 2D scans from such devices. We provide a proof of concept, that the registration with regard to all six degrees of freedom, i.e., unconstrained motion in 3D, is possible with data from 2D laser range finders (LRF).

To overcome the high ambiguity of the pose of single 2D scans, we consider a combination of two such scanners. We use two LRFs with different orientation on the same acquisition device. This means that the scans are pairwise rigidly coupled. An illustration is given in Figure 2. By the term *scan*, we will refer to such a combined scan pair in the remainder of the paper. In the illustrations, however, we will only show single scans in favor of a better understanding.

Common registration techniques that work on point data, such as variants of the Iterated Closest Point (ICP) algorithm or the Normal Distributions Transform (NDT) rely implicitly (ICP) or explicitly (NDT) on the fact that the captured points locally represent a smooth surface. Surfaces, however,

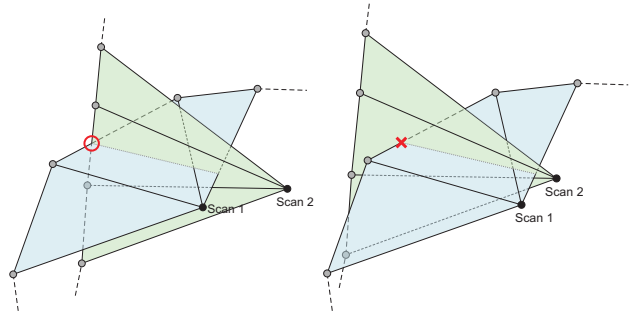


Figure 1. If we assume that triangles spanned by two neighbored scan points and the origin of the scan represent free space, then scans that do not comply with this rule indicate an incorrect registration. The proposed algorithm tries to resolve such intersections.

are not well captured in single 2D scans, therefore such algorithms are not directly applicable on the described type of data. The underlying idea of the algorithm proposed here, is to enforce the preservation of empty space. This means that we register the scans by resolving intrusions.

Assuming, the scans are densely sampled, then each line segment connecting two neighbored scan points together with the origin of the scan spans a triangle of free space. Two line segments of a pair of correctly registered scans therefore may intersect. However, if a line segment of one scan intersects the triangle of free space of another one, this indicates an incorrect registration of the scans (cf. Figure 1). In an iterative algorithm, we register the scans by applying rigid-body transformations that resolve these intersections.

We briefly discuss previous work related to the presented registration problem in the following section. In Section III the registration algorithm is described. In Section IV we discuss the simulation process of the range data that are used to investigate the algorithm. The results of the conducted experiments together with a short discussion are provided in Section V.

II. RELATED WORK

The registration of 3D point data with regard to six degrees of freedom is a well studied topic. The iterated closest point algorithm (ICP, [1], [2], [3]) is a very popular method that works well if the point clouds have significant overlap or the initial pose estimate is close to the solution.

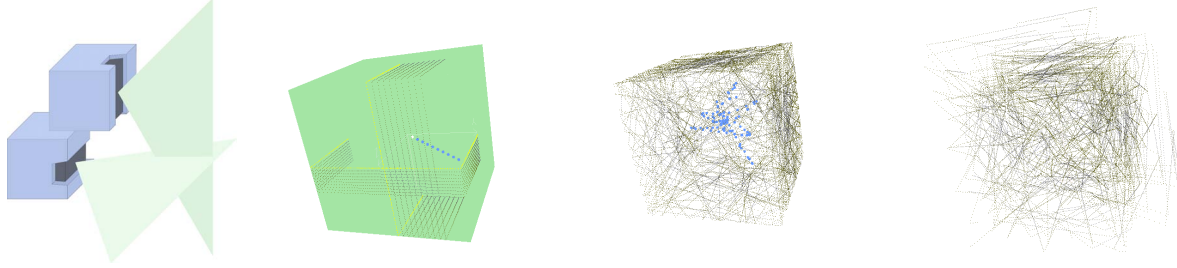


Figure 2. Illustration of the sensor setup and resulting scans (from left to right): **1.** Registered sequence of 10 scans of a cube model (purely linear motion, first scan highlighted). **2.** Registered sequence of 100 scans, acquired with the B-Spline motion model. Scan origins are depicted in blue. **3.** Same as 2, with position information discarded.

An alternative, that also works on 3D point data, is the normal distributions transform (NDT, [4]) which performs comparably [5].

Both methods were successfully used for the acquisition of 3D models using a stop-scan-go pattern of the sensor platform, e.g. in [6], [7], [8]. In the last few years, approaches to a more continuous form of 3D scanning (scanning while moving) were taken. Cole and Newman [9] presented a system that captures 3D data continuously using odometry information. They segment the data stream into chunks of smaller 3D point clouds and register these to improve the measured transformations. Additionally, a 2D SLAM technique is used since the motion is assumed to happen mostly in a horizontal plane. Harrison and Newman [10] presented another approach, where the idea is to correct the transformations such that vertical planes become exactly vertical. More recently, Stoyanov and Lilienthal [11] applied loop closure using ICP and a multi level relaxation scheme on 3D scans of a rotating 2D laser scanner.

Very good registration results have also been achieved by using feature points with descriptors based on 3D geometry (e.g. [12], [13]) or with descriptors derived from additionally available image data (e.g. [14], [15]).

In contrast to these approaches, we directly register single 2D scan lines and use a volumetric approach similar to the idea of space carving [16] in image based modeling. With this approach we allow full six degree of freedom motions as opposed to systems in the spirit of [17], where the acquisition device only moves in the horizontal plane.

III. RESOLVING INTERSECTIONS

Intersections of a scan line segment of a *reference scan* with triangles spanned by a line segment and the origin of an *intruder scan* indicate an inexact registration. This assumption holds true as long as the local sampling density is high, i.e., the scan line represents a line on the captured surface. In this case, the proposed algorithm tries to resolve all intersections by correcting the relative poses of the scans.

In order to reduce the computational complexity, the scans are simplified in a preprocessing step. We apply the Douglas-

Peucker [18] algorithm that approximates the scan by a subset of the points with a specified maximum error, which can be set according to the noise level of the range values.

Iteratively, the intersecting reference and intruder line segments are determined and the intrusions are minimized. The minimization problem can either be solved by a variational formulation or with a physically motivated approach. We use a mass-spring model where the springs are in state of rest when the intruding line segment intersects with the line segment of the reference scan, i.e. with one boundary of the reference triangle.

Note that the given problem, in general, is only solvable offline in batch-mode, also called *n-scan matching*, since smaller subsets of the scans (as used in an incremental registration) do not provide enough spatial constraints for a robust registration, because a sufficient sampling of the scene is necessary to align single 2D scan lines. It should, however, be possible to use the method to improve existing pre-registered models.

In the following we will describe some extensions to the model that are quite descriptive from the rigid body dynamics point of view. A well comprehensible introduction to the simulation of rigid body dynamics can be found in [19].

A. The Mass-Spring Model

At a single intersection, it is necessary to not only consider the involved reference and intruder line segment but to search for a nearest neighbor pair of line segments on the reference and intruder scan. Attaching a spring to these two closest line segments in the model means that we effectively minimize their distance. This way, the optimization tends to be less local which is mandatory when we are far from the solution. However, the radius of the nearest neighbor search around the intersection needs to be restricted when the expected remaining error becomes smaller. Otherwise, it could happen that out of two intersections of a scan pair, only one is effectively resolved (cf. Figure 3). We chose to couple the search radius r_{NN} to the maximum of the forces (see below) from the last iteration $r_{NN}^{(t)} = 2 \|\mathbf{F}_{max}^{(t-1)}\|_2$.

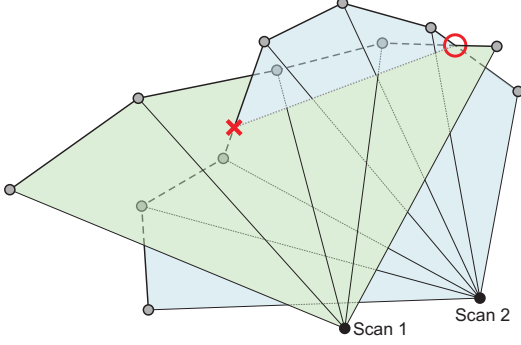


Figure 3. A scan pair that intersects twice. Here, a global nearest neighbor search is misleading. The intersection marked with "X" is never resolved since a segment pair with smaller distance (marked with a circle) is always found.

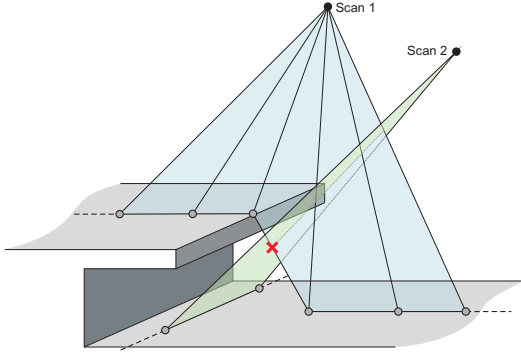


Figure 4. Intersections may occur not only due to misalignment, but also due to occlusions and undersampling.

In cases where the sampling density is rather low, or where parts of the scene are occluded in one scan, intersections may also occur when the scans are perfectly registered (cf. Figure 4). We therefore scale the spring rate

$$\kappa = \exp - \left(\frac{1}{3} \left| \frac{2\theta}{\pi} - 1 \right| \right)^2 \quad (1)$$

with regard to the scan angle θ of the intruder scan (cf. Figure 5). This results in a full application of the force, where the sampling density is maximal ($\theta = \pi/2$) and close to zero where the scan ray hits the surface in an acute angle ($\theta \approx 0$). Thus, we obtain the force $\mathbf{f} = \kappa \mathbf{d}$ that acts on both scans, where the vector \mathbf{d} denotes the distance of the line segments.

Each spring effects the reference and the intruder scan with the same force. Assuming that the scans have a certain weight, we can determine which scan should be effected more or less – equivalent to an elastic collision. The idea is to equip scans with a great mass if they already fit well into the 3D model. A good fit is indicated by many intersections with other scans that only induce minimal forces. In each iteration we compute a notional mass that linearly depends

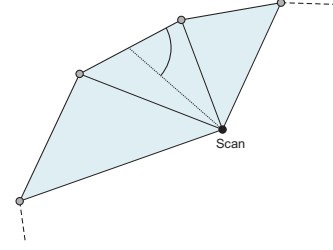


Figure 5. Scan angle θ . A small value indicates low sampling density and potential occlusions.

on the mean of the squared spring forces. Let \mathcal{I}_i denote the set of intersections, where the scan i is involved as either intruder or reference, so we obtain

$$m_i = \frac{|\mathcal{I}_i|}{\sum_{\ell \in \mathcal{I}_i} \|\mathbf{f}_i^{(\ell)}\|_2^2}. \quad (2)$$

Since the spring forces also produce a rotational movement, the distribution of the mass needs to be modeled as well for each scan. We chose to equally distribute the mass onto the scan points, which leads to an inertia tensor \mathbf{I} that has constant structure in the coordinate frame of the scan and only scales with the actual mass.

B. Solving the System

1) *Clustering Forces:* For a homogeneously sampled scene, it would be correct to sum up the forces of all springs $\mathbf{f}_i^{(\ell)}$, $\ell = 1, \dots, n$, connected to a scan i in order to compute the overall force acting on this scan. Since we are dealing with imperfectly sampled scenes, we need to decouple the simulation from the sampling process that produced the scans. From Figure 6 it can be observed that the force caused by a certain registration error scales with the number of intersections. We compensate for these repeated collisions by clustering forces with regard to their directions. For a set of cluster representatives \mathbf{c}_k , $k = 1, \dots, m$, by scaling the contribution to a cluster with the length of the projection

$$p_{i,k}^{(\ell)} = \left(\mathbf{f}_i^{(\ell)} \right)^\top \mathbf{c}_k, \quad (3)$$

we obtain an overall force acting on scan i ,

$$\mathbf{F}_i = \sum_k \frac{1}{Z_{i,k}} \left(\sum_{\ell} w_{i,k}^{(\ell)} p_{i,k}^{(\ell)} \right) \mathbf{c}_k, \quad (4)$$

with weights

$$w_{i,k}^{(\ell)} = \left| \frac{1}{\|\mathbf{f}_i^{(\ell)}\|_2} p_{i,k}^{(\ell)} \right| \quad (5)$$

and normalizer

$$Z_{i,k} = \sum_{\ell} w_{i,k}^{(\ell)}. \quad (6)$$

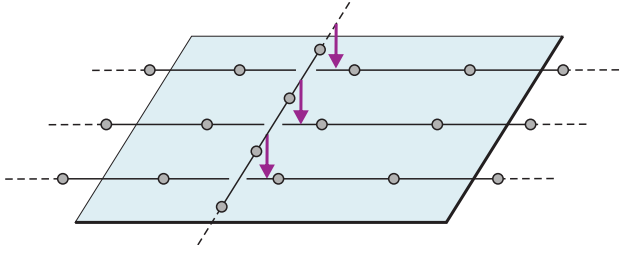


Figure 6. Coupling of sampling and simulation: Depending on the local sampling density, a constant registration offset induces a different number of instances of the same force.

Analogously, we compute the overall torque as

$$\tau_i = \sum_k \frac{1}{Z_{i,k}} \sum_{\ell} w_{i,k}^{(\ell)} p_{i,k}^{(\ell)} \mathbf{c}_k \times \mathbf{r}_i^{(\ell)}, \quad (7)$$

where $\mathbf{r}_i^{(\ell)}$ is the vector from the barycenter of the scan to the intersection point of the line segment with the reference triangle.

2) *Regularization*: In order not to get stuck in local minima and to improve the robustness of the method, we incorporate additional springs into the system, i.e., we apply external regularization forces. Let \mathbf{s}_i and \mathbf{q}_i denote the origin and the orientation (in quaternion representation) of scan i . From its neighbors in time, and based on the original orientation measurement $\tilde{\mathbf{q}}_i$, we compute a force

$$\mathbf{F}_i^{reg} = \frac{1}{2} (\mathbf{s}_{i-1} + \mathbf{s}_{i+1}) - \mathbf{s}_i, \quad (8)$$

and a torque

$$\tau_i^{reg} = \mathbf{I} \omega_i, \quad (9)$$

that are applied to each scan i . The angular velocity ω_i is computed as the axis-angle representation of the deviation from the orientation measurement $\mathbf{q}_{\Delta} = \mathbf{q}_i^{-1} \otimes \tilde{\mathbf{q}}_i$ (\otimes denoting quaternion multiplication).

Both, for the linear and angular regularization, we use a fixed spring rate starting at 1.0 and we anneal the system by lowering its value whenever the system meets a convergence criterion.

We solve the mass spring model with an explicit Euler method using a high damping constant. Note that such a solver is very similar to a steepest gradient descent of a variational least squares formulation of the problem. We experienced that a full minimization of the intrusions in one iteration of the algorithm is not preferable. This is due to the fact that the minimization problem very often changes from one iteration to the next, since different intersections occur. Apart from that, for the registration problem it is necessary that a great percentage of the scan pairs intersect. Methods that exploit the sparseness of a problem are therefore not applicable and a full minimization in each iteration would be very costly. Therefore, it is reasonable to only perform small

updates on the poses of the scans – as it is done with the explicit Euler method –, before evaluating the intersections once again.

A short summary of the iterative algorithm is given in Table I.

1. detect intrusions

- test all scans pairwise

2. search nearest neighbor line segments

- distances represent the forces via $\mathbf{f} = \kappa \mathbf{d}$

3. compute the scan masses

- cf. Equation 2

3. apply forces

- partition onto both scans (elastic collision)

- accumulate and normalize forces for each scan (Eq. 4)

- add regularization (Eqs. 8,9)

- perform one Euler step

goto 1.

Table I

BRIEF SUMMARY OF THE REGISTRATION ALGORITHM.

IV. THE DATA

For the investigation of the presented registration problem, we use simulated data for the experiments described in this paper. This means that we do not have to deal with time synchronization issues between the sensors. Furthermore, perfect ground truth data is available for quantifiable results and comparisons. The problem itself should, however, not be altered. Therefore, we employ a realistic sensor model that reproduces different real world error sources of the scanning process. The sensor model and the motion model, i.e. assumptions on how the sensors are moved through the scene while recording, are described in the following subsection.

The virtual assembly of the scanners is as described in Section I and is depicted in Figure 2.

The registration process is started with an initial guess of the orientation for each scan, e.g. this could be provided by an additional IMU. Accordingly, we apply random noise to the ground truth orientation (uniformly distributed axes and normally distributed angles).

A. Simulating the Acquisition

The acquisition of the range data is simulated by computing scan ray distances to the mesh-based 3D test models. To account for the systematic and the statistic errors of the sensor, in direction as well as in range, we add Gaussian noise to the depth values ($\sigma = 1.0\text{cm}$). Furthermore, we simulate the effect of *flying pixels*, that occurs whenever the spot of the scan ray covers surfaces at different distance as it happens on edges of objects. We use Monte Carlo integration with 50 samples of the scan cone and restrict the

| Name | # vertices | dimensions [m] | # scans | # control points |
|----------------|------------|-------------------------------|---------|------------------|
| Living Room | 72,791 | $8 \times 7.5 \times 3.2$ | 300 | 75 |
| Lab | 125,805 | $20.9 \times 6.5 \times 3.2$ | 300 | 75 |
| Roman Temple 1 | 190,227 | $21.5 \times 15 \times 9.5$ | 300 | 30 |
| Roman Temple 2 | | | 300 | 75 |
| Office | 269,039 | $25.5 \times 16.8 \times 8.6$ | 300 | 75 |
| Kyoto Shelter | 1,547 | $4.5 \times 4.3 \times 4.5$ | 200 | 20 |

Table II
SIMULATED DATA SETS.

integration area to the length of the measurement impulse. The maximum range of the scanner is taken into account, i.e. measurements where less than half of the samples hit a surface of the model, are marked as *max range* readings. The choice of parameters is exemplarily based on the specifications of the *SICK LMS200* range finder [20], [21].

The linear motion of the sensor is modeled with a B-Spline curve that interpolates randomly chosen control points in 3D. For the rotation of the sensor, we use the same interpolation applied in the exponential chart [22], i.e., the axis-angle representation, relative to the first control point of the respective interval. The control points of the quaternion curves represent random orientations, i.e. two consecutive control points may have completely different orientation.

Assuming a motion with moderate speed and a LRF working at high frequency, the ego-motion during the acquisition of single 2D scans is neglected.

V. EXPERIMENTS

We tested our algorithm on various data sets. Figure 7 gives an impression of the scenes and Table II lists the specifications of the 3D models as well as the simulated scan data.

A. Implementation and Settings

Due to the computational load of the algorithm, we compute the nearest neighbor search and the distances of the line segments in a brute-force implementation on the GPU, which has shown much better performance than a CPU-based solution using diverse hierarchical data structures.

In all experiments the registration starts with orientation values that are obtained by perturbing the correct orientation by noise with standard deviation $\sigma = 3^\circ$ (see Section IV). The position information is completely discarded, i.e. all scans are reset to the scene origin. To account for this disparity of the errors, we decrease the torque in the mass spring model by an additional factor of 0.3 with regard to the translational step size.

For the normalization (Eq. 4), we achieved the best results when using an arbitrarily oriented basis of three orthogonal cluster representatives.

The annealing scheme applied to the regularization leads to increased run times of the algorithm, yet contributes considerably to its robustness. We use the non-monotony of

the sum of squared forces $\sum_i \|\mathbf{F}_i\|_2^2$ as convergence criterion and, each time it is met, we decrease the spring rate by a factor of 1.2.

The simulated acquisition processes in the tests are of two different types: For the first one (*Roman Temple 1, Kyoto Shelter*), we used smooth B-Spline curves for the trajectories as well as for the course of the orientation by choosing a low ratio of control points to number of scans. In the second mode (*Living Room, Lab, Roman Temple 2, Office*), the speed of the motion and of the change of orientation varies drastically due to a high number of control points. We run this second simulation in order to validate that a successful registration is also possible when the underlying assumptions of the regularization and the actual motion differ significantly.

B. Results

The quantitative reconstruction results are shown in Table III and different views of the resulting point clouds are presented in Figures 8 and 9, as well as in the supplementary video.

As a measure for the quality of the reconstruction one can look at the remaining offset of the scan origin and its orientation. In certain configurations, however, there is no unique correct pose for the scan, e.g. it can be translated along a certain direction without altering the model quality. Additionally, offsets in position and orientation can compensate each other to some degree. Therefore, in Table III, we present the average and the maximum point-to-surface distance (PSD), i.e. the distance of each scan point to the nearest triangle of the mesh. Note that noise and flying pixels lead to a non-zero PSD also for the perfectly registered ground truth models.

Additionally, the sum of squared distances (SSD) of the reconstructed scanner positions is provided, since based on the PSD, large offsets may be underestimated. This is due to the fact that the association of a point and the originally captured surface is not taken into account.

Especially, the *Roman Temple* and the *Kyoto Shelter* scenes were chosen as very challenging scenes, yet both are registered precisely. In the first one, the occlusions from the columns are obviously well handled by scaling the spring rate with regard to the scan angle (cf. Eq. 1). In the latter one, the simulated LRF returns a large amount of invalid

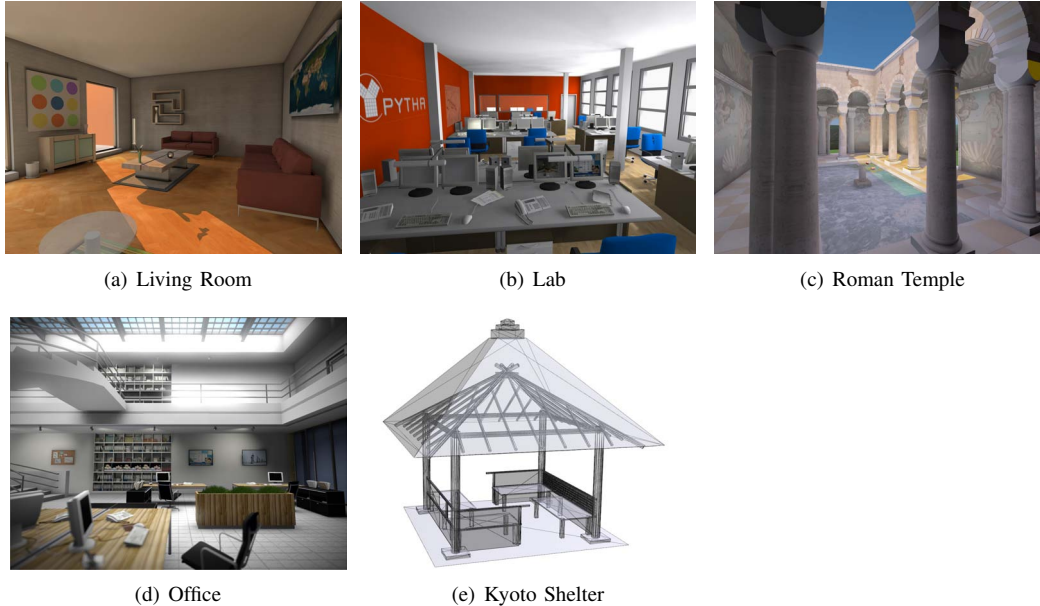


Figure 7. Virtual Scenes used for the simulation.

| Name | # iterations | SSD (initial) | PSD (initial) | PSD (ground truth) | PSD (reconstr.) | SSD (reconstr.) |
|----------------|--------------|---------------|-----------------|--------------------|------------------|-----------------|
| Living Room | 3289 | 58.30 | 0.16 (max 1.09) | 0.005 (max 0.17) | 0.011 (max 0.22) | 0.54 |
| Lab | 3123 | 51.00 | 0.16 (max 1.46) | 0.004 (max 0.29) | 0.012 (max 0.53) | 0.89 |
| Roman Temple 1 | 7939 | 205.5 | 0.31 (max 1.99) | 0.004 (max 0.12) | 0.007 (max 0.56) | 0.07 |
| Roman Temple 2 | 8162 | 45.79 | 0.15 (max 1.74) | 0.004 (max 0.11) | 0.013 (max 1.64) | 0.87 |
| Office | 4364 | 58.30 | 0.16 (max 1.77) | 0.004 (max 0.18) | 0.022 (max 2.48) | 0.39 |
| Kyoto Shelter | 2166 | 25.24 | 0.08 (max 0.62) | 0.004 (max 0.16) | 0.006 (max 0.21) | 0.08 |

Table III

REGISTRATION RESULTS. THE BARYCENTER AND THE AVERAGE ORIENTATION OF THE SCANS OF THE RECONSTRUCTION AND INITIAL CONFIGURATION ARE ALIGNED TO GROUND TRUTH BEFORE EVALUATION.

range readings, since a major part of the shelter is open. However, the model is successfully reconstructed with a precision close to the original noise level.

Obviously, the robustness of the registration depends on the coverage of the scans. Invariably, it can happen that a few scans (often < 10) are registered less exact and contribute heavily to the overall error. This can happen due to insufficient constraints imposed by the surrounding scans, especially when the sampling in the acquisition process was not dense enough. Or, depending on the structure of the scene, scans get stuck in local minima during optimization. Therefore, it should be helpful to integrate an outlier detection step of some sort and to discard single perturbing scans during registration. As additional experiments with manually removed outliers have shown, this can lead to a significantly improved overall performance, while losing only a marginal amount of information about the scene.

VI. CONCLUSION

We presented a novel algorithm that allows us to register single pairs of 2D scans with regard to six degrees of

freedom, which is achieved by using a volume-oriented method that resolves mutual intrusions of the scans. This is in contrast to popular algorithms, like ICP or NDT, that maximize the congruence of the captured surfaces. It is feasible to apply this algorithm and to solve this novel registration problem due to the increased performance of modern hardware, and mainly due to a fast, GPU-based implementation.

Based on simulated data, the paper presents a first proof of concept with promising results. The acquisition process is modeled carefully, yet we will further investigate the applicability of the proposed algorithm to the acquisition of real scenes. To achieve good results, it may be necessary to extend the preprocessing of the range data with regard to noise and it might help to explicitly handle single perturbing scans.

ACKNOWLEDGMENT

We thank Philipp Jenke for some very fruitful discussions. The authors gratefully acknowledge financial support by the German Research Foundation (DFG).

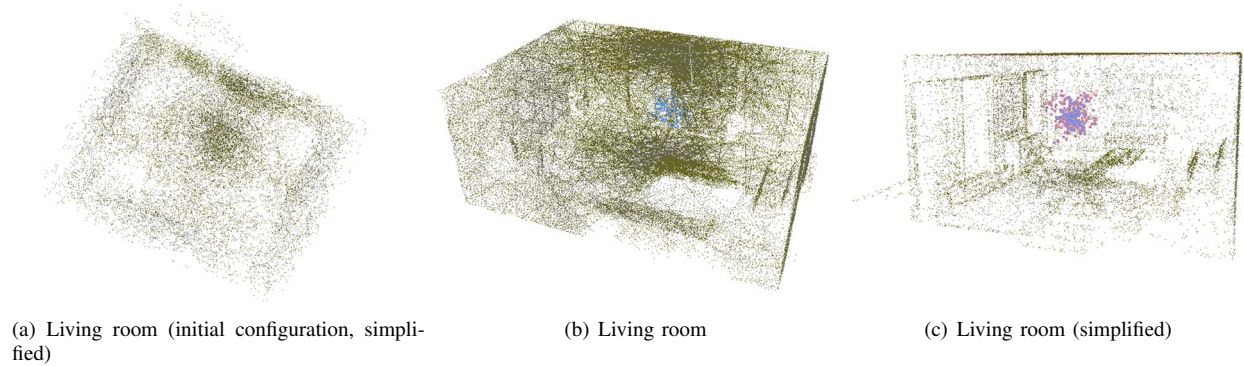


Figure 8. Reconstructed Point Clouds. Blue and red dots indicate the reconstructed scan origins. The *simplified* version of the point clouds is the same as is used for the registration.

REFERENCES

- [1] P. J. Besl and N. D. McKay, "A method for registration of 3-d shapes," *IEEE Transactions on Pattern Analysis and Machine Intelligence (PAMI)*, vol. 14, no. 2, pp. 239–256, 1992.
- [2] Y. Chen and G. Medioni, "Object modelling by registration of multiple range images," *Image and Vision Computing*, vol. 10, no. 3, pp. 145–155, Apr. 1992.
- [3] S. M. Rusinkiewicz, "Efficient variants of the ICP algorithm," in *Proceedings of the International Conference on 3-D Digital Imaging and Modeling (3DIM)*, 2001, pp. 145–152.
- [4] P. Biber and W. Straßer, "The Normal Distributions Transform: A New Approach to Laser Scan Matching," in *Proc. IEEE/RSJ International Conference on Intelligent Robots and Systems (IROS)*, 2003.
- [5] M. Magnusson, A. Nüchter, C. Lörken, A. J. Lilienthal, and J. Hertzberg, "Evaluation of 3D Registration Reliability and Speed – A Comparison of ICP and NDT," in *Proc. of IEEE International Conference on Robotics and Automation (ICRA)*, 2009.
- [6] H. Surmann, A. Nüchter, and J. Hertzberg, "An autonomous mobile robot with a 3D laser range finder for 3D exploration and digitalization of indoor environments," *Robotics and Autonomous Systems*, vol. 45, pp. 181–198, 2003.
- [7] A. Nüchter, H. Surmann, K. Lingemann, J. Hertzberg, and S. Thrun, "6D SLAM with Application in Autonomous Mine Mapping," in *Proc. ICRA '04*, 2004, pp. 1998–2003.
- [8] M. Magnusson, T. Duckett, and A. J. Lilienthal, "3d scan registration for autonomous mining vehicles," *Journal of Field Robotics*, vol. 24, no. 10, pp. 803–827, Oct 24 2007.
- [9] D. M. Cole and P. M. Newman, "Using Laser Range Data for 3D SLAM in Outdoor Environments," in *Proc. of IEEE International Conference on Robotics and Automation (ICRA)*, 2006.
- [10] A. Harrison and P. Newman, "High Quality 3D Laser Ranging Under General Vehicle Motion," in *Proc. IEEE International Conference on Robotics and Automation (ICRA)*, Pasadena, California, April 2008.
- [11] T. Stoyanov and A. J. Lilienthal, "Maximum likelihood point cloud acquisition from a mobile platform," in *Proc. Int. Conf. on Advanced Robotics (ICAR)*, 2009.
- [12] A. E. Johnson, "Spin images: A representation for 3-D surface matching," Ph.D. dissertation, Carnegie Mellon University, 1997.
- [13] N. Gelfand, N. J. Mitra, L. J. Guibas, and H. Pottmann, "Robust global registration," in *Symposium on Geometry Processing (SGP)*, 2005.
- [14] G. H. Bendels, P. Degener, R. Wahl, M. Körtgen, and R. Klein, "Image-Based Registration of 3D-Range Data Using Feature Surface Elements," in *Proc. Int. Symposium on Virtual Reality, Archaeology and Cultural Heritage (VAST)*, 2004.
- [15] H. Andreasson and A. J. Lilienthal, "6D Scan Registration using Depth-Interpolated Local Image Features," *Robotics and Autonomous Systems*, vol. 58, no. 2, 2010.
- [16] K. N. Kutulakos and S. M. Seitz, "A Theory of Shape by Space Carving," *International Journal of Computer Vision*, vol. 38, no. 3, pp. 199–218, 2000.
- [17] C. Früh and A. Zakhor, "Constructing 3D City Models by Merging Ground-Based and Airborne Views," in *Proc. IEEE Conference on Computer Vision and Pattern Recognition (CVPR)*, 2003.
- [18] D. Douglas and T. Peucker, "Algorithms for the reduction of the number of points required to represent a digitized line or its caricature," *The Canadian Cartographer*, vol. 10, pp. 112–122, 1973.
- [19] D. Baraff, "An introduction to physically based modeling: Rigid body simulation i – unconstrained rigid body dynamics," in *SIGGRAPH Course Notes*, 1997.
- [20] *Telegram Listing*, SICK AG, Waldkirch, Germany, 2006.
- [21] *Technical Description*, SICK AG, Waldkirch, Germany, 2006.
- [22] X. Pennec, "Computing the mean of geometric features – application to the mean rotation," Institut National de Recherche en Informatique et en Automatique, Tech. Rep., 1998.

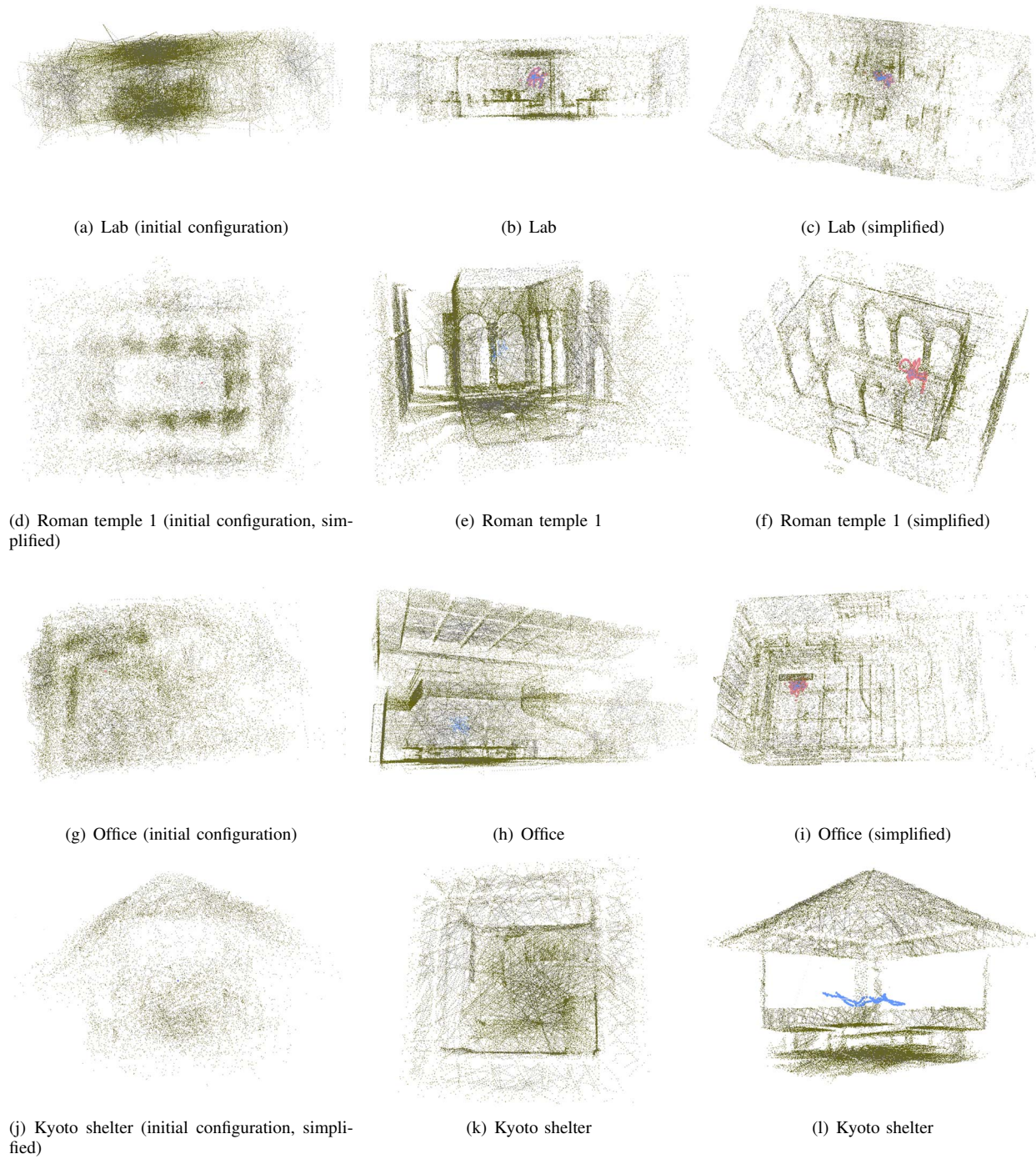


Figure 9. Reconstructed Point Clouds, continued.